

Electronic Supplementary Information

**Coupling of Electrocatalytic CO₂ Reduction and CH₄ Oxidation for
Efficient Methyl Formate Electrosynthesis**

Quan Zhang,^a Yangshen Chen,^a Shuai Yan,^a Ximeng Lv,^a Chao Yang,^a Min Kuang,^{b,*} and
Gengfeng Zheng^{a,*}

^a Laboratory of Advanced Materials, Department of Chemistry and Shanghai Key Laboratory of Molecular Catalysis and Innovative Materials, Fudan University, Shanghai 200438, China

^b State Key Laboratory for Modification of Chemical Fibers and Polymer Materials, College of Materials Science and Engineering, Donghua University, Shanghai 201620, China.

*Address correspondence to: gfzheng@fudan.edu.cn (G.Z.) or mkuang@dhu.edu.cn (M.K.)

Experimental

Chemicals

$\text{Bi}(\text{NO}_3)_3 \cdot 5\text{H}_2\text{O}$, ethylene glycol, and NaBH_4 were purchased from Sigma-Aldrich. $\text{IrCl}_3 \cdot x\text{H}_2\text{O}$, NaNO_3 , and cysteamine·HCl were purchased from Sinopharm Chemical Reagent Co., Ltd. All the chemicals were used as received without further purification.

Synthesis of Bi catalysts

The Bi catalysts were synthesized with a reduction method.^{S1} Typically, 0.1 g of $\text{Bi}(\text{NO}_3)_3 \cdot 5\text{H}_2\text{O}$ (0.2 mmol) was added into 50 mL of ethylene glycol solution. The solution was sonicated for 30 min, and continuously stirred for 2 h. Subsequently, the suspension was transferred into a Teflon-lined autoclave and heated at 180 °C for 12 h. The product was collected and dispersed in 50 mL of fresh NaBH_4 solution (10 mM), and then kept stirring for 12 h. The black precipitate was filtered, washed with distilled water and ethanol. The Bi catalysts were finally obtained after drying at 80 °C under vacuum.

Synthesis of IrO_2 catalysts

The IrO_2 catalysts were synthesized according to an Adams fusion.^{S2} In brief, 100 mg of $\text{IrCl}_3 \cdot x\text{H}_2\text{O}$, 2 g of NaNO_3 , and 50 mg of cysteamine·HCl were dissolved in 5 mL of deionized (DI) water. The solution was kept stirring for 1 h at 80 °C, and then transferred to a convection oven at 80 °C to evaporate redundant water. The dried powder was collected with finely ground, and then transferred to an alumina crucible. The calcination procedure was performed at 450 °C for 90 min with a heating rate of 3 °C min^{-1} . The samples were cooled to room temperature, and thoroughly washed with copious amounts of deionized water. Finally, the obtained IrO_2 catalyst was used after drying under vacuum overnight.

Materials characterization

The crystal structures of the as-synthesized catalysts were measured using a X-ray diffraction (XRD) spectrometer (D8 Advance, Bruker Corp., Germany). The material morphologies were characterized using a transmission electron microscope (TEM, JEM-2011, JOEL, Japan). The surface chemical state and composition were analyzed using X-ray photoelectron spectroscopy (XPS, Thermo Scientific K-Alpha, USA) with Al K α radiation, and all binding energies were calibrated to C 1s peak (284.6 eV) for a reference.

Electrochemical measurements

The electrochemical CO₂ reduction was measured using a gas diffusion layer (GDL) loaded Bi catalyst as the cathode, a IrO₂-loaded GDL as the anode, and an anion exchange membrane (AEM, FAB-PK-130, Fumatech) to separate the cathode and anode chambers. Both the catholyte and anolyte were 0.5 M KOH aqueous solution with a flow rate of 20 mL·min⁻¹ using a peristaltic pump. The reactant CO₂ gas was pumped into the cathode, and the flow rate was controlled at ~ 40 mL·min⁻¹ by a gas flow meter. There was no reactive gas entering the anode side, so only oxygen evolution reaction (OER) took place. An electrochemical station (Reference 3000, Gamry Instruments) was used to perform the electrochemical measurement, which was carried out in a three-electrode system, and the reference electrode was located in the cathode side. All scan rates used in the LSV studies were 50 mV s⁻¹. The electrode potentials were converted into reversible hydrogen electrode by the equation:

$$E (\text{vs. RHE}) = E (\text{vs. Ag/AgCl}) + 0.197 \text{ V} + 0.059 \times \text{pH}.$$

The electrochemical CH₄ oxidation was measured using a gas diffusion layer (GDL) loaded with IrO₂ as the anode, a GDL loaded with Bi catalyst as the cathode, and an anion exchange membrane (AEM, FAB-PK-130, Fumatech) to separate the cathode and anode chambers. The anolyte was a mixture of 1 M KCl aqueous solution and 0.5 M KOH aqueous

solution in a flow rate of $\sim 20 \text{ mL}\cdot\text{min}^{-1}$ using a peristaltic pump, where the aqueous KOH allowed to increase the solubility of gaseous CH_3Cl product. The catholyte was used with 0.5 M KOH aqueous solution in a flow rate of $\sim 20 \text{ mL}\cdot\text{min}^{-1}$ using a peristaltic pump. The reactant CH_4 gas was pumped into the anode, and the flow rate was controlled at $\sim 40 \text{ mL}\cdot\text{min}^{-1}$ by a gas flow meter. There was no reactive gas entering the cathode side, so only hydrogen evolution reaction took place. An electrochemical station (Reference 3000, Gamry Instruments) was used to perform the electrochemical measurement, which was carried out in a three-electrode system, and the reference electrode was located in the anode side. All scan rates used in the LSV studies were 50 mV s^{-1} . The electrode potentials were converted into reversible hydrogen electrode by the equation:

$$E (\text{vs. RHE}) = E (\text{vs. Ag/AgCl}) + 0.197 \text{ V} + 0.059 \times \text{pH}.$$

In an integrated tandem reaction cell, the simultaneous CO_2RR and CH_4OR operation steps were performed as follows:

The integrated tandem reaction cell was consisted of electrodes and anion exchange membrane (AEM). The cathode electrode was prepared by a deposition method. In brief, 5 mg of Bi catalyst was dispersed in 1.0 mL of isopropanol, with 50 μL of 5 wt% Nafion added afterwards. The mixture was sonicated and sprayed on a carbon gas-diffusion layer (GDL) substrate. The anode electrode was assembled in a similar way, using 5 mg of the as-synthesized IrO_2 as the catalyst. The electrochemical CO_2 reduction and CH_4 oxidation were simultaneously conducted in the integrated tandem reaction cell. Similarly, a gas diffusion layer (GDL) loaded with IrO_2 was chosen as the anode, a GDL loaded with Bi catalyst was used as the cathode, and an anion exchange membrane (X37-50 grade 60, Sustainion, Dioxide materials) to separate the cathode and anode chambers. The area specific resistance (ASR) of model “X37-50 grade 60” was much lower than the resistance of model “FAB-PK-130”, benefiting larger current densities under the same voltage conditions. The anolyte was a

mixture of 1 M KCl aqueous solution and 0.5 M KOH aqueous solution in a flow rate of $\sim 20 \text{ mL}\cdot\text{min}^{-1}$ using a peristaltic pump, where the aqueous KOH benefited the solubility of gaseous CH_3Cl product. The catholyte was used with 0.5 M KOH aqueous solution in a flow rate of $\sim 20 \text{ mL}\cdot\text{min}^{-1}$ using a peristaltic pump. The reactant CH_4 and CO_2 gases were pumped into the anode and cathode, respectively, and the flow rates were controlled at $\sim 40 \text{ mL}\cdot\text{min}^{-1}$ by a gas flow meter. An electrochemical station (Reference 3000, Gamry Instruments) was used to perform the electrochemical measurement, which was carried out in a three-electrode system, and the reference electrode was located in the anode side. All scan rates used in the LSV studies were 50 mV s^{-1} . The electrode potentials were converted into reversible hydrogen electrode by the equation:

$$E (\text{vs. RHE}) = E (\text{vs. Ag/AgCl}) + 0.197 \text{ V} + 0.059 \times \text{pH}.$$

The Faraday efficiency (FE) of chlorine (Cl_2) was determined by a standard iodometry method.^{S3} In brief, the anode electrolyte was taken into an iodine flask containing KI (20 wt%) and H_2SO_4 (0.5 wt%) after electrolyzing for a period of time. The color of the solution changed to blue when the starch indicator solution (1 wt%) was added into the iodine flask. Finally, the blue mixture was titrated using a calibrated $\text{Na}_2\text{S}_2\text{O}_3$ solution (0.05 mol L^{-1}) until the color disappeared. The FE of Cl_2 evolution (CIER) was then calculated by the equation:

$$\text{FE}_{\text{Cl}_2} = \frac{2 \times F \times c \times V}{It} \times 100\%$$

where the number “2” denotes the two-electron transfer number, F is the Faraday constant (96485 C mol^{-1}), c is the concentration of Cl_2 (mol L^{-1}), V is the volume of the electrolyte solution (L), I is the current (A), and t represents the electrolysis time (s).

The Faraday efficiency (FE) of CH_3Cl evolution reaction was calculated by the equation:

$$\text{FE}_{\text{CH}_3\text{Cl}} = \frac{n \times m \times F}{Q} \times 100\%$$

where n is the number of transferred electrons, m is the amount of produced CH_3Cl products,

F is the Faraday constant (96485 C mol⁻¹), and Q is the quantity of applied electric charges during the chronoamperometric measurements.

The Faraday efficiency (FE) of oxygen reaction (O₂) was calculated by the equation:

$$FE_{O_2} = \frac{n \times m \times F}{Q} \times 100\%$$

where n is the number of transferred electrons, m is the amount of O₂ products, F is the Faraday constant (96485 C mol⁻¹), and Q is the quantity of applied electric charges during the chronoamperometric measurements.

Determination of products

The gas products of CH₃Cl were qualitatively analyzed by an on-line gas chromatograph (GC 6600, Shanghai Fanwei Inc., China) equipped with a flame ionization detector (FID). The gas products of O₂ were determined by an on-line gas chromatography (GC 6600, Shanghai Fanwei Inc., China) using a thermal conductivity detector (TCD) detector. The liquid products were quantified by ¹H nuclear magnetic resonance (NMR, Bruker Advance 500, Germany).

In the quantitative determination of CH₃Cl products, due to the easy hydrolysis of CH₃Cl into methanol in alkaline electrolyte, the amounts of methanol should also be counted for total CH₃Cl. Thus, three kinds of products, including gaseous CH₃Cl, liquid HCOOCH₃, and liquid CH₃OH should be added together to quantify the actual yields of CH₃Cl products.

Calculation of energy efficiency (EE):^{S4-S7}

For a cathodic CO₂RR in a cell reactor:

$$EE_{\text{cathode}} = \frac{E^0}{-E_{\text{full-cell applied}}} FE = \frac{E_{OER} - E_{CO_2RR}}{-E_{\text{full-cell applied}}} FE_{\text{formate}} = \frac{1.23 - (-0.12)}{-(-3.6)} * 80\% = 30\%$$

where E_{OER} is the standard potential for anodic oxygen evolution reaction (i.e., 1.23 V), $E_{\text{CO}_2\text{RR}}$ is the thermodynamic potential of CO_2 electroreduction to formate (i.e., -0.12 V), FE_{formate} is the faradaic efficiency of electrocatalytic CO_2 -to-formate (i.e., 80%) and $E_{\text{full-cell applied}}$ is the applied full-cell voltage (that is, 3.6 V).

For an anodic CH_4OR in another cell reactor:

$$EE_{\text{anode}} = \frac{E^0}{E_{\text{full-cell applied}}} FE = \frac{E_{\text{CH}_4\text{OR}} - E_{\text{HER}}}{E_{\text{full-cell applied}}} FE_{\text{CH}_3\text{Cl}} = \frac{1.49 - 0}{3.6} * 34\% = 14.1\%$$

where $E_{\text{CH}_4\text{OR}}$ is the standard potential for methane oxidation reaction (i.e., 1.49 V), E_{HER} is the thermodynamic potential of H_2O electroreduction to hydrogen (i.e., 0 V), $FE_{\text{CH}_3\text{Cl}}$ is the faradaic efficiency of electrocatalytic CH_4 -to- CH_3Cl (i.e., 34%), and $E_{\text{full-cell applied}}$ is the applied full-cell voltage (i.e., 3.6 V).

We combine this two-cell reactor to produce the value-added methyl formate (see **Figure S12**). Since the synthesis of methyl formate from CH_3Cl with HCOO^- is a non-Faraday process, we assume that there is no energy loss in this procedure. So, the energy waste can be traceable to the electrocatalytic CO_2 -to-formate and CH_4 -to- CH_3Cl reaction. Thus, the energy efficiency can be calculated:

$$EE = EE_{\text{cathode}} * EE_{\text{anode}} = 30\% * 14.1\% = 4.2\%$$

The coupling of CO_2RR and CH_4OR in an integrated tandem reaction cell:

As the anodic CH_4OR is dynamically unfavorable than the cathodic CO_2RR , hence the EE value was calculated with the $FE_{\text{CH}_4\text{OR}}$ as a reference when coupling CO_2RR and CH_4OR in an integrated tandem reaction cell:

$$EE = \frac{E^0}{E_{\text{full-cell applied}}} FE = \frac{E_{\text{CH}_4\text{OR}} - E_{\text{CO}_2\text{RR}}}{E_{\text{full-cell applied}}} FE_{\text{CH}_3\text{Cl}} = \frac{1.49 - (-0.12)}{3.6} * 34\% = 15.2\%$$

where $E_{\text{CH}_4\text{OR}}$ is the standard potential for CH_4 oxidation reaction (i.e., 1.49 V), $E_{\text{CO}_2\text{RR}}$ is the thermodynamic potential of CO_2 electroreduction to formate (i.e., -0.12 V), $FE_{\text{CH}_3\text{Cl}}$ is the

Faradaic efficiency of electrocatalytic CH₄-to-CH₃Cl (i.e., 34%), and $E_{\text{full-cell applied}}$ is the applied cell voltage (that is, 3.6 V).

Computational methods

The density functional theory (DFT) calculations were carried out using the *Vienna Ab initio* Simulation Package (VASP).^{S8} The electron-ion interaction was represented by the projector augmented wave (PAW), and the kinetic energy cutoff of plane wave was set as 400 eV. The PBE functional was utilized for geometry optimization.^{S9-S10} The gamma-centered ($3 \times 2 \times 1$) k-point mesh for IrO₂, and gamma-centered ($2 \times 2 \times 1$) k-point mesh for Bi catalysts were utilized to calculate the electronic structure, and a vacuum slab with 15 Å thickness was considered. During optimization, the top two atomic layers were fully relaxed until the residual force was less than 0.02 eV·Å⁻¹. The Gibbs free energy (ΔG) was evaluated by adding corrections from zero-point energy (ZPE) and vibrational entropy (S), which can be written as:

$$\Delta G = \Delta E_{\text{DFT}} + \Delta \text{ZPE} - T\Delta S$$

For the adsorbed species, ZPE and S were derived by frequency calculations with the harmonic oscillator approximation, and the VASPKIT code for post-processing of calculated data was adopted.^{S11}

The quantum chemistry calculations for explaining the nucleophilic reaction of HCOO⁻ or OH⁻ with CH₃Cl were finished by DFT embedded in Gaussian 16 program package. The B3LYP exchange-correlation functional^{S12} in cooperation with 6-31G* basis set^{S13} was utilized for geometry optimization, frequency analysis and energy determination.

Supplementary Figures

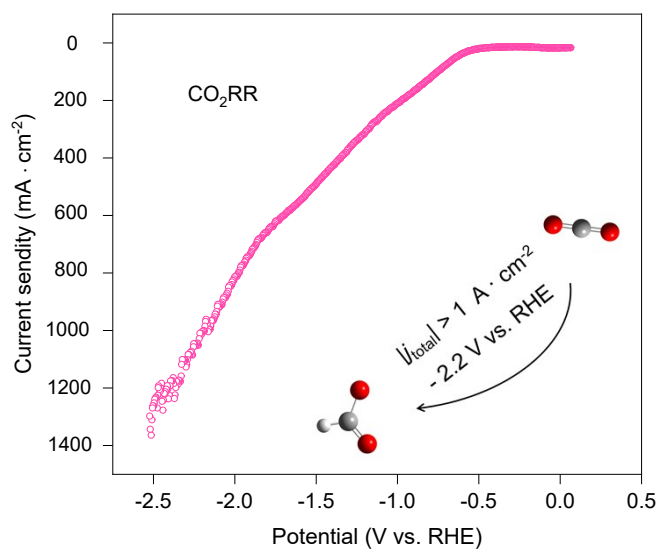


Figure S1. LSV curve of Bi catalysts in 0.5 M KOH electrolyte with flowed CO₂.

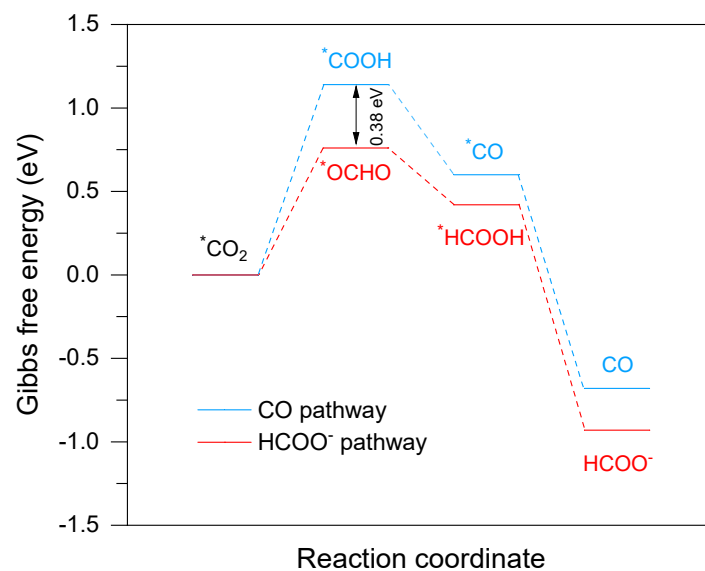


Figure S2. Gibbs free energy diagrams of CO₂ reduction to HCOO⁻ and CO products on the (012) crystal surface of the Bi electrocatalyst.

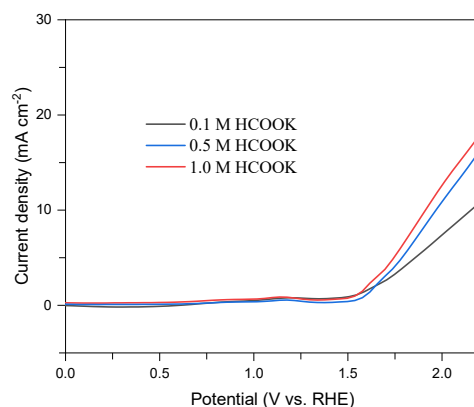


Figure S3. LSV curves of aqueous HCOOK in electrolyte of KCl (1 M) and KOH (0.5 M) over IrO₂ electrocatalysts in a H-cell. Results indicated a typical OER process with an initial potential at ~1.48 V vs. RHE, suggesting the non-oxidized HCOO⁻ in the anodic region.

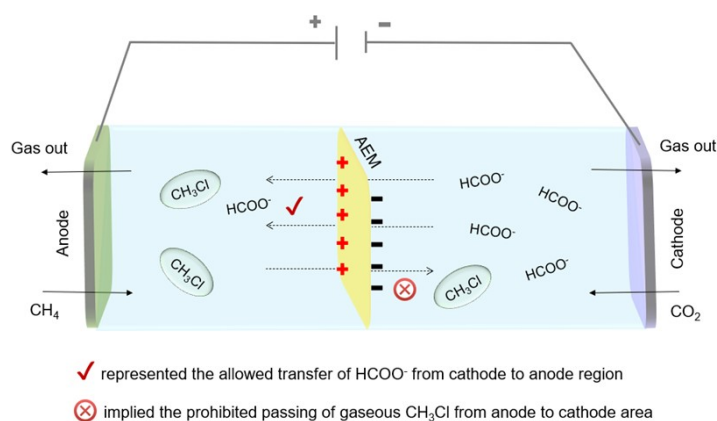


Figure S4. The allowed transfer of HCOO⁻ and prohibited passing of CH₃Cl by the anion exchange membrane (AEM) under electric field. There was a gas outlet designed on anodic side of the electrochemical cell, and the generated CH₃Cl was more inclined to be discharged from the gas outlet rather than overcoming the resistance of the AEM to penetrate into cathode area for coupling reactions. While the situation was different for HCOO⁻, as it existed in an aqueous form, thus endowing the transfer into anodic part under the electric field.

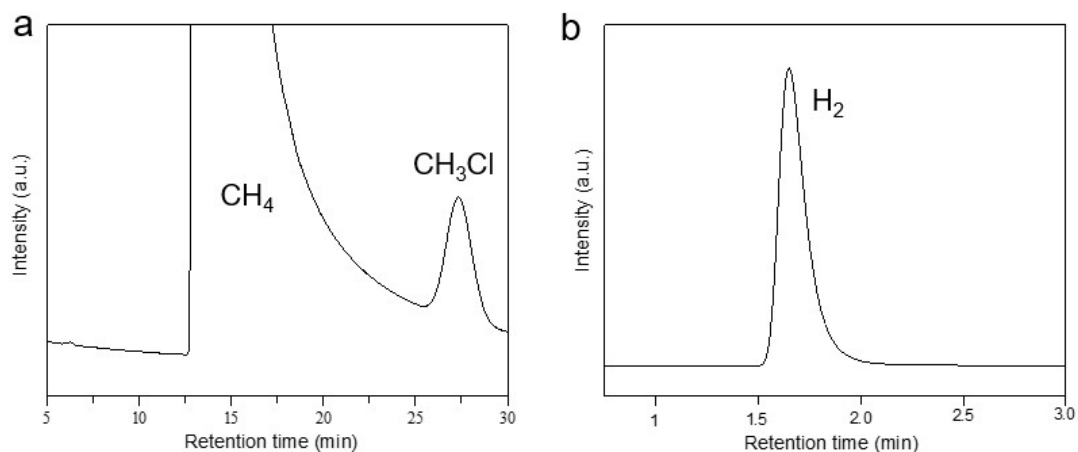


Figure S5. Detection of gaseous products from anodic and cathodic area. The anode was injected with methane for oxidization, while no gas was injected into the cathode (i.e., a typically HER process). As shown in Figure S5, the CH₃Cl product was found in the anode, while no signal of CH₃Cl was observed in cathode, confirming that CH₃Cl produced in anodic side were not transferred into the cathodic region for coupling reactions.

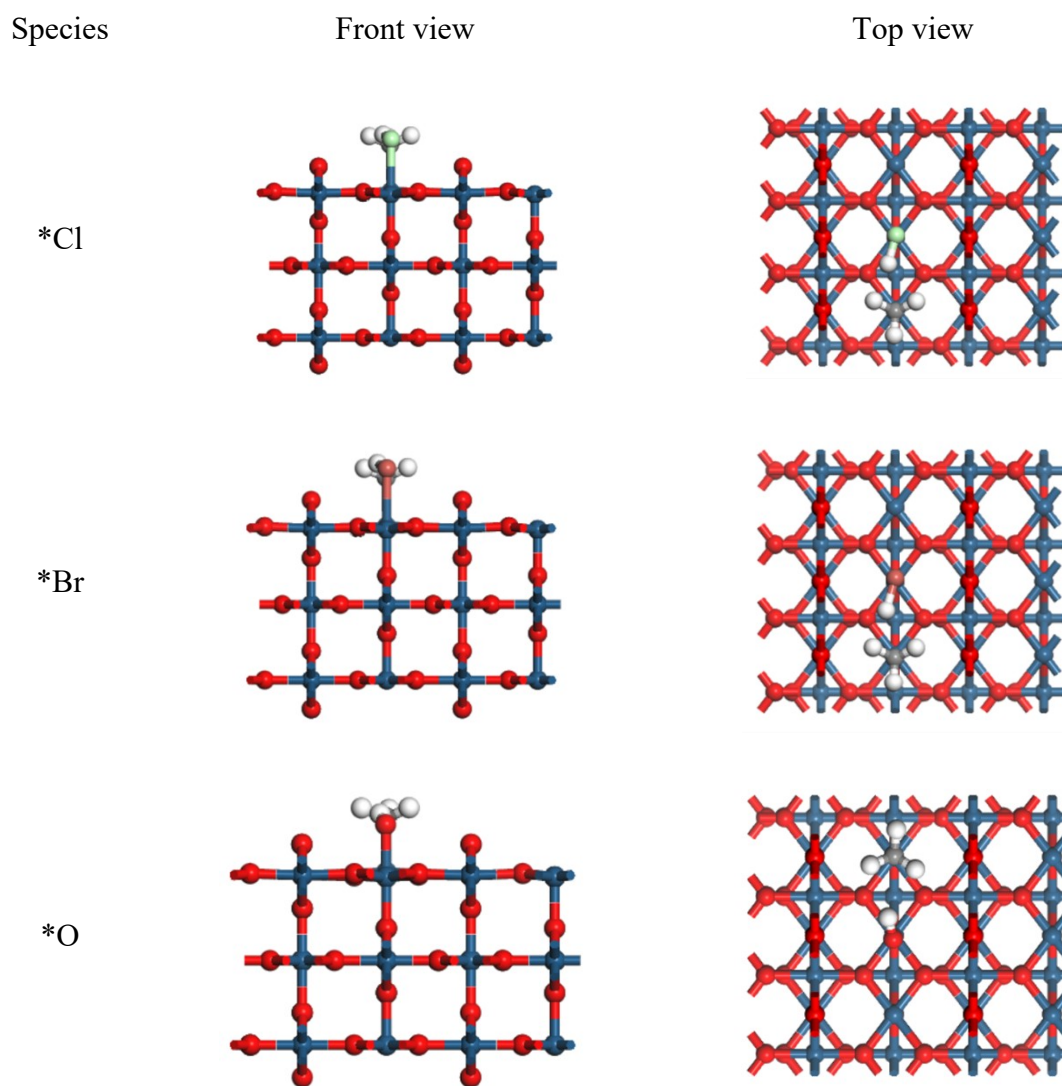


Figure S6. The optimized structure with functionalized *Cl, *Br, and *O (as representatives) for activating CH₄ into *CH₃ over IrO₂(110) surface.

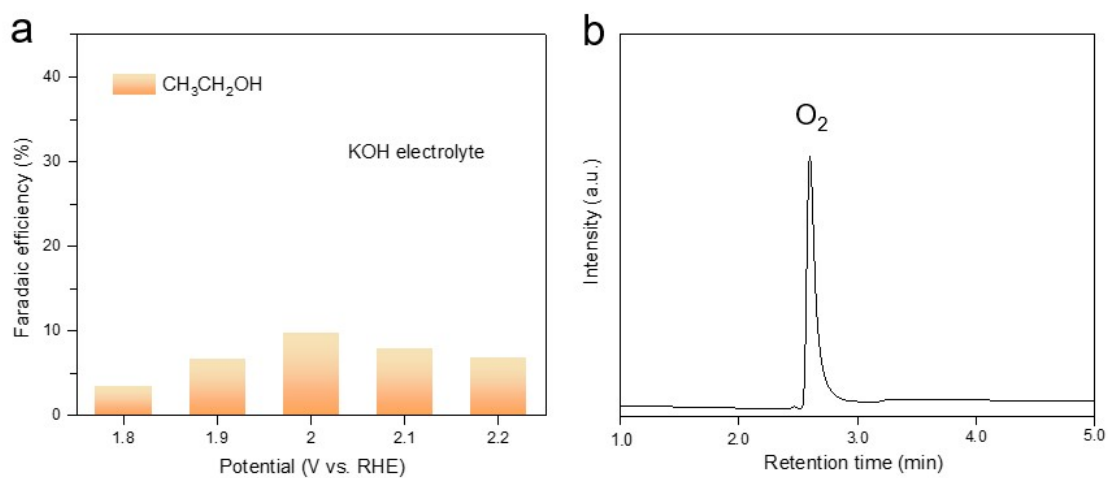


Figure S7. (a) Faradaic efficiency of the ethanol product in KOH electrolyte under different applied potentials, and (b) the determination of O_2 product using a TCD detector.

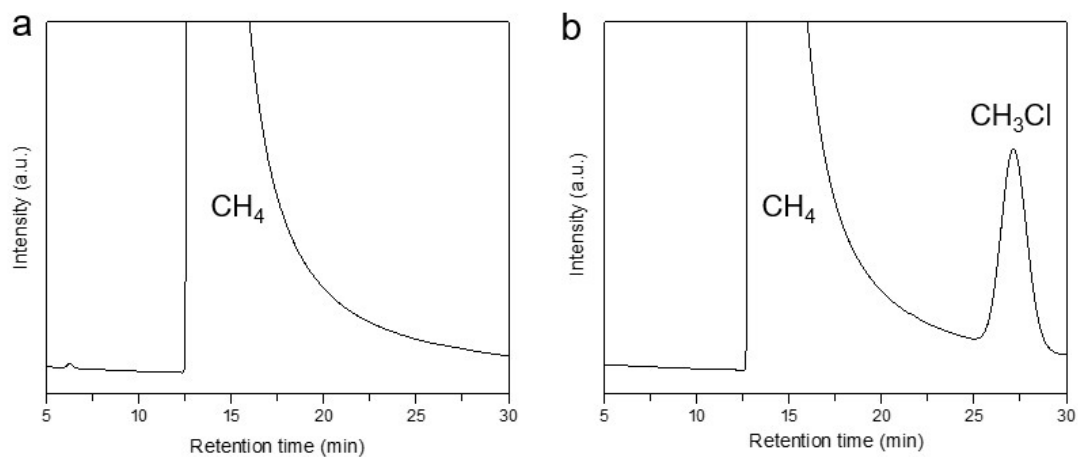


Figure S8. Signal of products during electrochemical CH_4 oxidization using a FID detector. (a) before, and (b) after the CH_4 oxidation reaction.

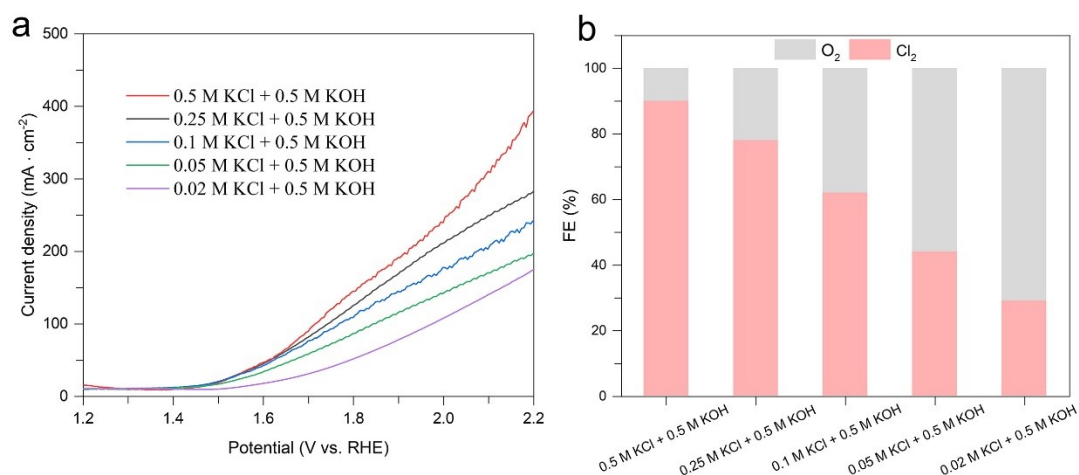


Figure S9. (a) LSV curves tested in 0.5 M aqueous KOH, with the decreased concentration of aqueous KCl from 0.5 to 0.02 M without the methane feed. (b) FE values of O₂ and Cl₂ products under an applied potential of 2.2 V vs. RHE. The gradient experiments by electrolyzing the changeable concentration of KCl were carried out in a mixed KCl and KOH electrolytes, where the concentration of aqueous KOH was fixed at 0.5 M. The concentration of KCl should not exceed one tenth of KOH, otherwise the major product was still Cl₂. Moreover, the required numbers of transferred electrons to yield Cl₂ from Cl⁻ are 2 ($2\text{Cl}^- \rightarrow \text{Cl}_2 + 2\text{e}^-$), while 4 electrons are needed to transfer from OH⁻ to O₂ ($4\text{OH}^- \rightarrow \text{O}_2 + 2\text{H}_2\text{O} + 4\text{e}^-$), suggesting anionic Cl⁻ is more dynamically favored to be oxidized than the OH⁻.

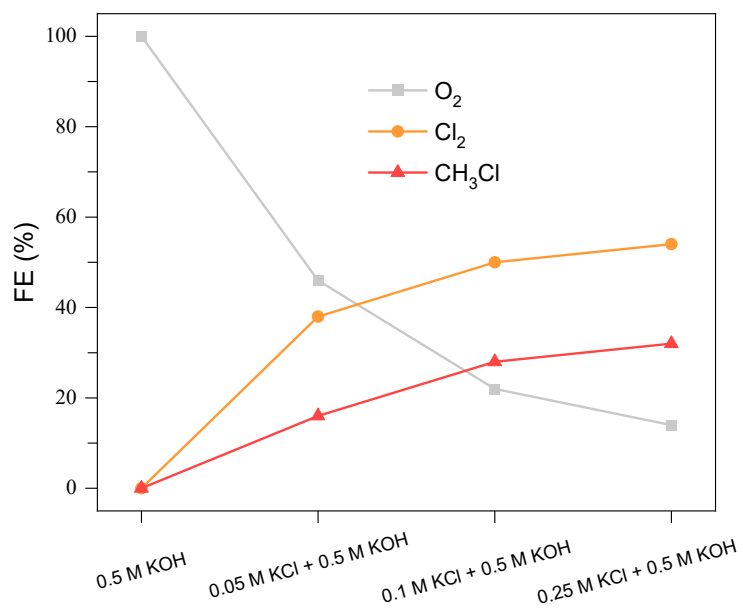


Figure S10. FE values of gases products by controlling the concentration of aqueous KCl from 0 to 0.25 M in a mixed electrolyte of KCl with KOH (0.5 M) with the methane feed. The applied potential was 2.2 V *vs.* RHE. The FEs of Cl₂ and CH₃Cl both increased with the increased concentrations of aqueous KCl electrolyte. However, no CH₃Cl signals was detected when aqueous KCl electrolyte was absent, implying the chlorination evolution reaction promoted methane oxidation into CH₃Cl.

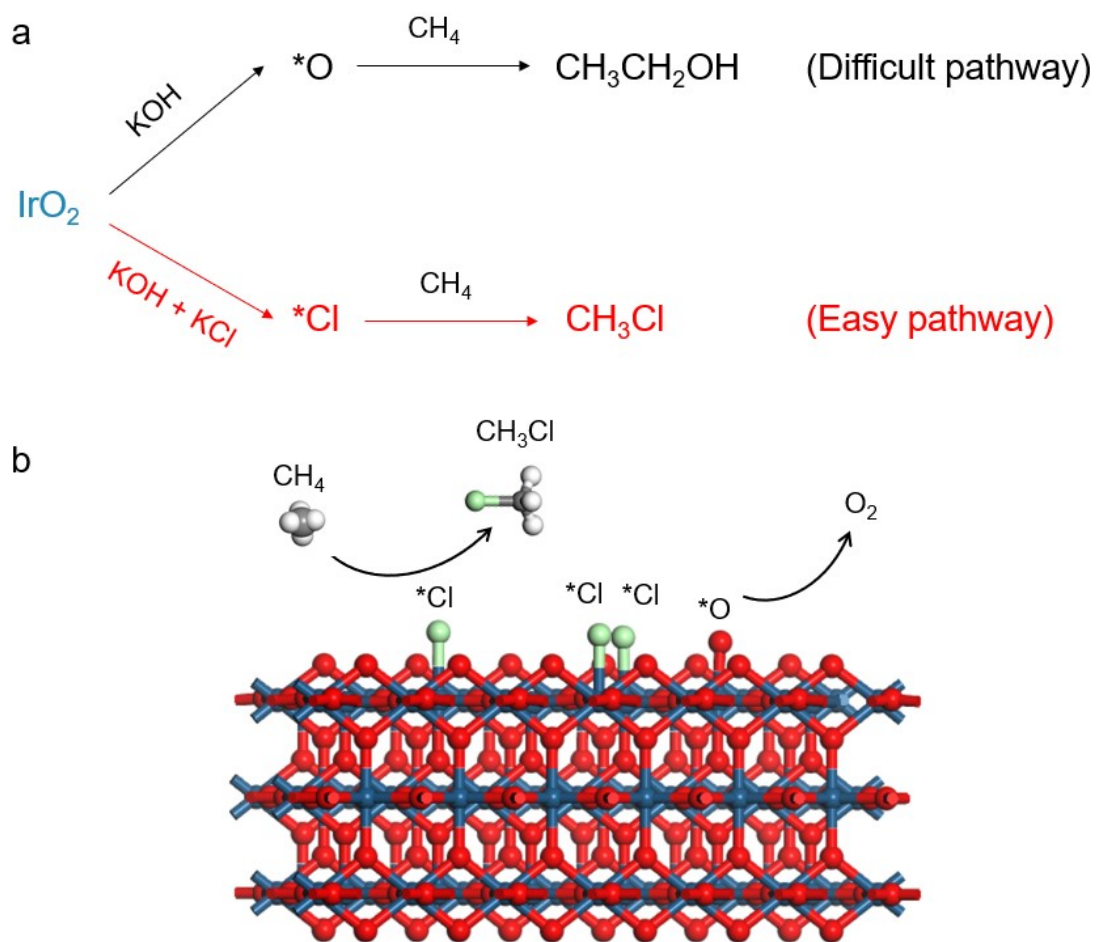


Figure S11. (a) Summary conversion pathways of CH_4OR in aqueous KOH and mixed KOH with KCl electrolyte over IrO_2 catalysts. (b) The exhibition of absorbed $^*\text{Cl}$ species suppressed the occupation of $^*\text{O}$ species on the surface of IrO_2 electrocatalysts, and thus the OER was significantly inhibited by CIER.

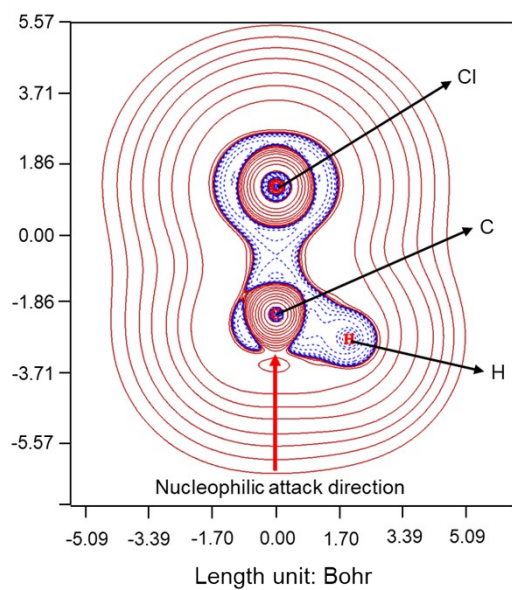


Figure S12. The Laplacian transform of the electron density of CH_3Cl molecules. Electrons diverged in the direction were indicated by the red arrow, suggesting the back position of carbon atom in CH_3Cl was more susceptible to nucleophilic attacks by OH^- or HCOO^- .

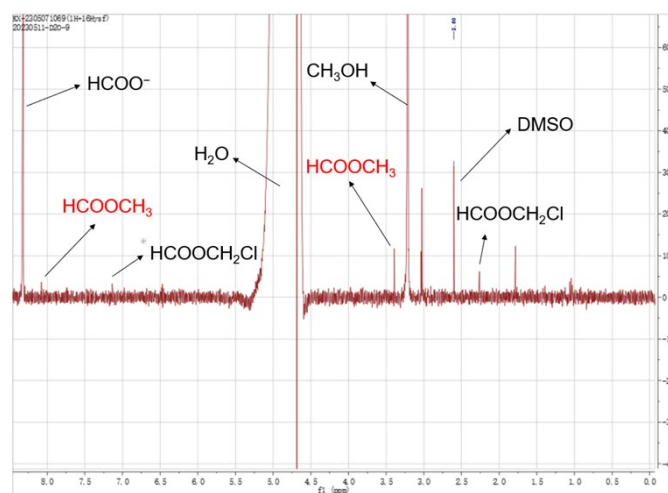


Figure S13. Representative ^1H -NMR spectrum of the liquid products.

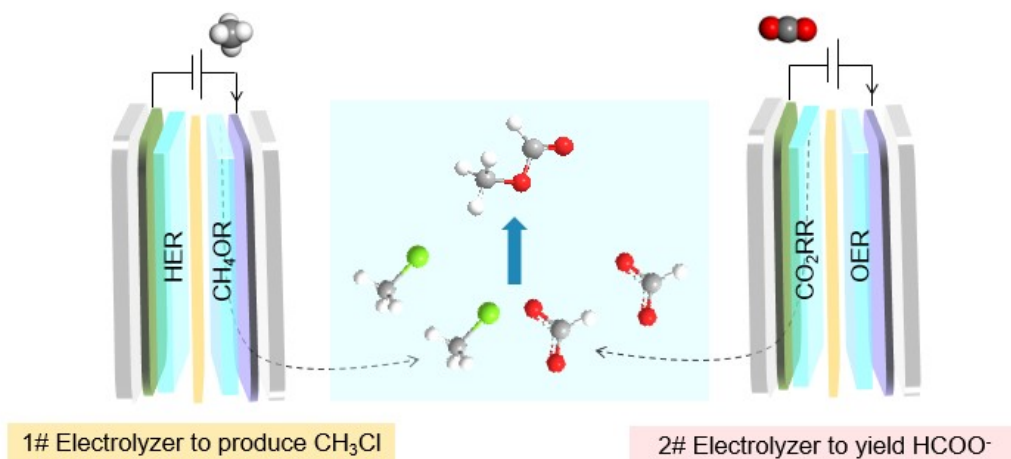


Figure S14. Electrosynthesis of methyl formate in two separated electrolyzers.

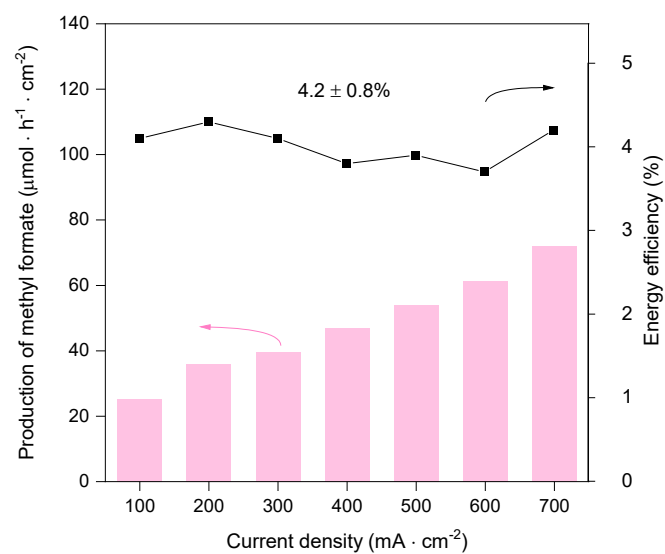


Figure S15. Methyl formate production and energy efficiencies in two separate electrolyzers.

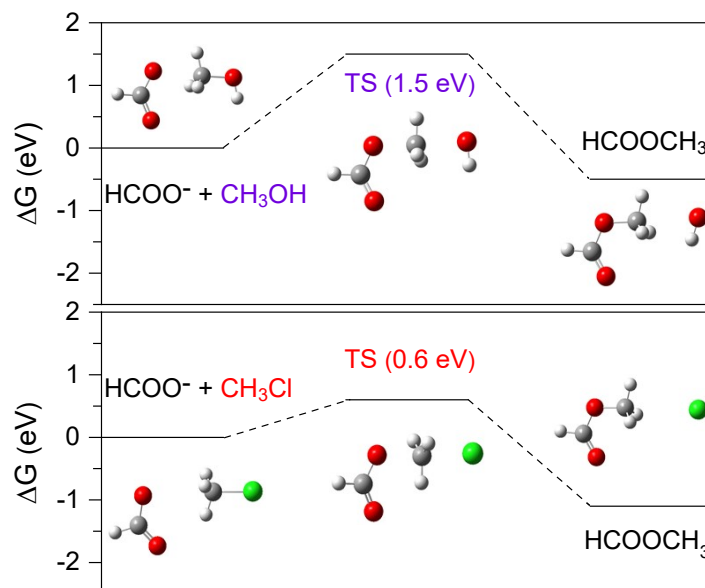


Figure S16. The calculated nucleophilic reaction pathways between HCOO^- with CH_3OH (top), and HCOO^- with CH_3Cl (bottom). The energy barrier in the reaction between HCOO^- with CH_3OH ($\Delta G = 1.5 \text{ eV}$) is higher than that between HCOO^- with CH_3Cl ($\Delta G = 0.6 \text{ eV}$), suggesting the more stable of CH_3OH than that of CH_3Cl to couple with HCOO^- for producing methyl formate.

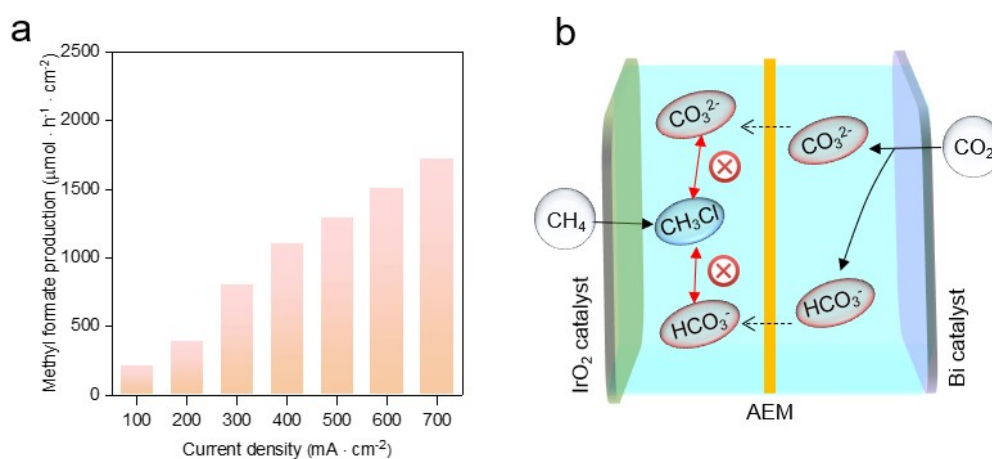


Figure S17. (a) Electrosynthesis of methyl formate in aqueous of KCl (1 M) and KOH (0.5 M) with simultaneous addition of aqueous KHCO_3 (0.005 M) and K_2CO_3 (0.005 M) electrolytes. (b) Illustration of the unavailable coupling of bicarbonate or carbonate ions with CH_3Cl .

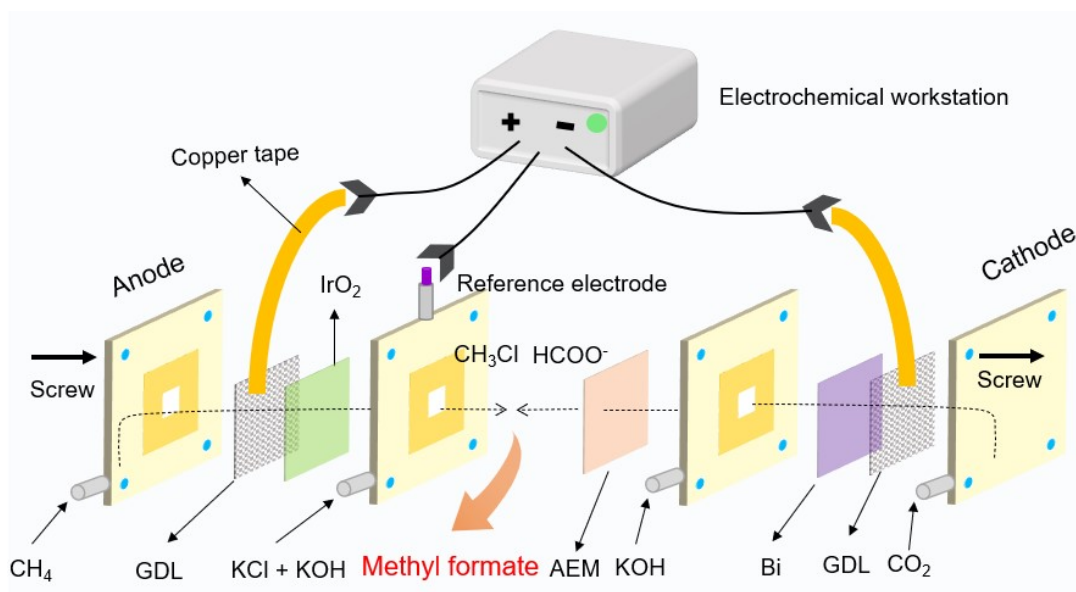


Figure S18. The combined CO₂RR and CH₄OR as the cathode and anode reactions in an electrochemical cell to electro-synthesize methyl formate. This tandem reaction cell (length * width = 7 cm * 7cm) was tightly assembled, and connected to an electrochemical workstation by sticking GDL with copper tapes. The CH₄ gases entered the reactor from the anodic side and diffused to the three-phase interface (CH₄-IrO₂-electrolyte) to yield CH₃Cl products. Similarly, the CO₂ gases entered the reactor from the cathodic side and also diffused to the three-phase interface (CO₂-Bi-electrolyte) to yield formate products during electrocatalysis. As the cathode and anode were simultaneously fed with reactant gases, a balanced gas flow rate of CO₂ and CH₄ (~ 40 mL·min⁻¹) on both sides was adopted to maintain the stability of CO₂ reduction and CH₄ oxidation reactions, respectively. On this occasion, the CH₄ inlet pressure was estimated to be 1.7 bar, and the CO₂ inlet pressure was controlled to be 1.6 bar.

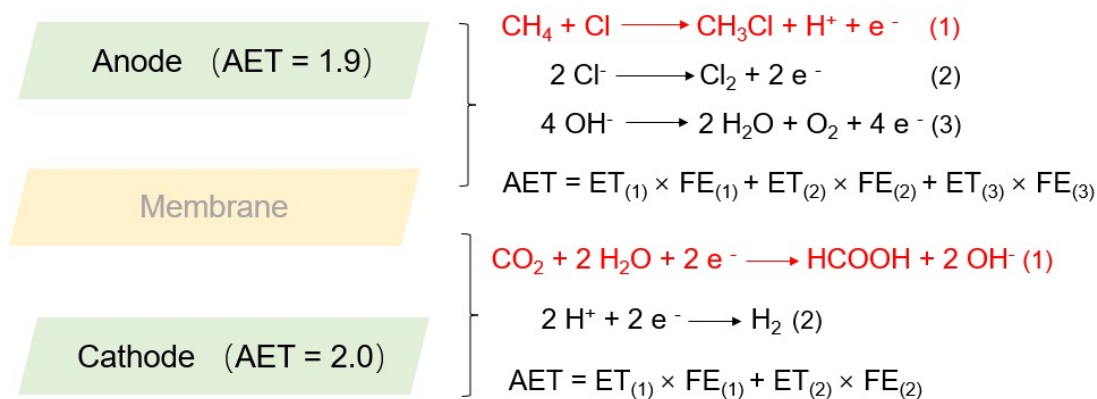


Figure S19. The average electron transfer (AET) numbers in anode and cathode reactions.

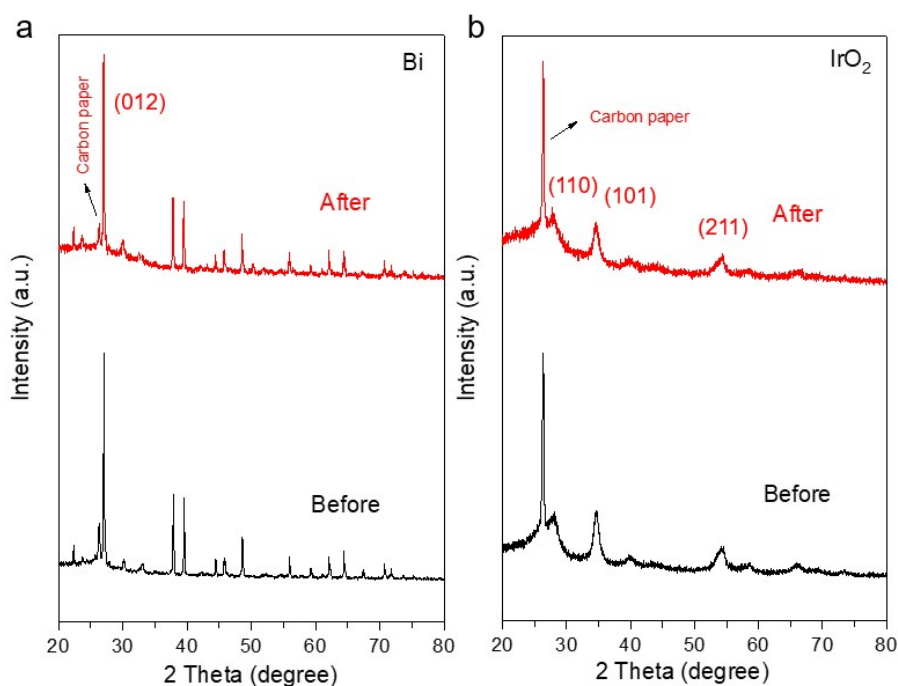


Figure S20. (a) XRD patterns of Bi-loaded GDL as the cathode, and (b) IrO₂-loaded GDL as the anode before and after electrocatalytic reactions under a current density of 700 mA cm⁻². The comparison of Bi and IrO₂ electrolysts before and after the electrolysis suggested the well-retained crystal structure after electrocatalytic reactions under a current density of 700 mA cm⁻².

References

- S1 X. Ma, J. Tian, M. Wang, M. Shen, and L. Zhang, *J. Colloid Interf. Sci.*, 2022, **608**, 1676.
- S2 J. Lim, D. Park, S. S. Jeon, C.-W. Roh, J. Choi, D. Yoon, M. Park, H. Jung, and H. Lee, *Adv. Funct. Mater.*, 2018, **28**, 1704796.
- S3 J. Hu, H. Xu, X. Feng, L. Lei, Y. He, and X. Zhang, *ChemElectroChem*, 2021, **8**, 1204.
- S4 F. Li, A. Thevenon, A. Rosas-Hernández, Z. Wang, Y. Li, C. Gabardo, A. Ozden, C. Dinh, J. Li, Y. Wang, J. Edwards, Y. Xu, C. McCallum, L. Tao, Z.-Q. Liang, M. Luo, X. Wang, H. Li, C. O'Brien, C.-S. Tan, D.-H. Nam, R. Quintero-Bermudez, T.-T. Zhuang, Y. Li, Z. Han, R. Britt, D. Sinton, T. Agapie, J. Peters, and E. Sargent, *Nature*, 2020, **577**, 509.
- S5 J. Jin, J. Wicks, Q. Min, J. Li, Y. Hu, J. Ma, Y. Wang, Z. Jiang, Y. Xu, R. Lu, G. Si, P. Papangelakis, M. Shakouri, Q. Xiao, P. Ou, X. Wang, Z. Chen, W. Zhang, K. Yu, J. Song, X. Jiang, P. Qiu, Y. Lou, D. Wu, Y. Mao, A. Ozden, C. Wang, B. Xia, X. Hu, V. Dravid, Y.-M. Yiu, T.-K. Sham, Z. Wang, D. Sinton, L. Mai, E. Sargent, and Y. Pang, *Nature*, 2023, **617**, 724.
- S6 X. Wang, Z. Wang, F. Pelayo García de Arquer, C.-T. Dinh, A. Ozden, Y. Li, D.-H. Nam, J. Li, Y.-S. Liu, J. Wicks, Z. Chen, M. Chi, B. Chen, Y. Wang, J. Tam, J. Howe, A. Proppe, P. Todorović, F. Li, T.-T. Zhuang, C. Gabardo, A. Kirmani, C. McCallum, S.-F. Hung, Y. Lum, M. Luo, Y. Min, A. Xu, C. O'Brien, B. Stephen, B. Sun, A. Ip, L. Richter, S. Kelley, D. Sinton, and E. Sargent, *Nat. Energy*, 2020, **5**, 478.
- S7 W. Lai, Y. Qiao, J. Zhang, Z. Lin, and H. Huang, *Energy Environ. Sci.*, 2022, **15**, 3603.
- S8 G. Kresse, J. Furthmüller, *Phys. Rev. B*, 1996, **54**, 11169.
- S9 V. Anisimov, J. Zaanen, O. Andersen, *Phys. Rev. B*, 1991, **44**, 943.
- S10 J. Perdew, K. Burke, M. Ernzerhof, *Phys. Rev. Lett.*, 1996, **77**, 3865.
- S11 V. Wang, N. Xu, J.-C. Liu, G. Tang, W.-T. Geng, *Comput. Phys. Commun.*, 2021, **267**, 108033.
- S12 A. Becke, *J. Chem. Phys.*, 1992, **96**, 2155.
- S13 P. Redfern, P. Zapol, L. Curtiss, K. Raghavachari, *J. Phys. Chem. A*, 2000, **104**, 5850.